https://doi.org/10.1016/j.carbon.2017.06.011

Ultra-broadband Frequency Responsive Sensor Based on Lightweight and Flexible Carbon Nanostructured Polymeric Nanocomposites

Zhihui Zeng[a,b,c,‡], *Menglong Liu*[a,‡], *Hao Xu*[a,‡], *Yaozhong Liao*[a], *Feng Duan*[b,c], *Li-min Zhou*[a], *Hao Jin*[b,*], *Zhong Zhang*[b,*], *and Zhongqing Su*[a,*]

[a] Department of Mechanical Engineering, The Hong Kong Polytechnic University, Kowloon, Hong Kong SAR

[b] CAS Key Laboratory of Nanosystem and Hierarchical Fabrication, CAS Center for Excellence in Nanoscience, National Center for Nanoscience and Technology, Beijing 100190, P. R. China

[c] School of Materials Science and Engineering, Nanyang Technological University, 50 Nanyang Avenue, Singapore 639798, Singapore

**Corresponding authors*

[‡]These authors contributed equally to this work.

Abstract: Strain sensing in an ultra-broadband frequency regime up to 400 kHz is obtained with developed lightweight and flexible carbon nanostructured polymer composites, in a frequency range far broader than any piezoresistive sensor previously reported. Various loadings, from static and low-frequency cyclic stretches, through high-frequency vibration, to ultrahigh-frequency ultrasonic guided waves, are applied for evaluation of the sensors' performance. Diverse content and type of carbon nanofiller, microstructure of the conductive network in the matrix, and

* Corresponding author. E-mail address: zhongqing.su@polyu.edu.hk (Z. Su); zhong.zhang@nanoctr.cn (Z. Zhang); hjin@nanoctr.cn (H. Jin).

electromechanical responses of the nanocomposites under broadband frequency strain are discussed, in conjunction with dynamic mechanical analysis and a theoretical nanoscale model, to advance insight into the sensing mechanism of the sensors. Implementation of ultrasonic guided wave-based *in-situ* structural health monitoring using networked sensors made of carbon black/polyvinylidene fluoride nanocomposites indicates the significant application potential of the developed sensor to serve as an ultra-broadband and high-frequency-responsive flexible strain sensor.

Keywords: ultra-broadband response; nanocomposite sensor; high-frequency piezoresistivity, Carbon black, MWCNT.

1 Introduction

Sensors play a rudimentary but critical role in collecting ambient and system information such as strain, stress/pressure, light, or temperature [1-3]. In particular, flexible strain sensors have stimulated growing demand for applications including wearable/portable electronics, artificial skin, soft robots, human-machine interfaces, human motion detection, and health monitoring of human or objective structures [4-8].

The achievement of desirable mechanical strength, low stiffness, high sensitivity (i.e., high gauge factor (GF)), a wide sensing range, and fast response to dynamic motion, along with a simple and low-cost fabrication process is always desirable but also challenging during strain sensor development [4, 9-10]. For example, a kind of crack-based strain sensor composed of a platinum (Pt) and rubber substrate inspired by the spider was developed recently, showing an ultrasensitive

response with a GF over 2000 [1]. Aligned single-walled carbon nanotubes attached on silicone rubber were designed as flexible strain sensors and demonstrated the capacity to measure strains up to 280% with a GF of 0.82, highlighting the potential of the sensor for the detection of human motion including movement, breathing, and speech [2]. Reduced graphene oxide/polyimide (PI) composite aerogels, fabricated by a simple approach based on freeze casting and thermal annealing, have exhibited low density, high flexibility and super-elasticity, endowing sensors with remarkable compression sensitivity and excellent durable stability [6]. Wearable and highly sensitive graphene woven microfabric-based flexible strain sensors, produced with a high GF and adjustable strain range, have highlighted the applicability of such sensors for detecting high-frequency sound signals [5, 8, 11].

In the past decade, in pursuit of different strain-sensing performance to accommodate various applications, numerous flexible strain sensors made of functional nanomaterials and polymer have been developed based on a variety of fabrication techniques and working mechanisms [12-15]. The nanomaterials, exhibiting outstanding electrical, mechanical, optical, and chemical properties, together with supporting polymers featuring flexibility, lightness, human-friendliness, and durability, have endowed nanocomposite sensors with advantages over conventional strain sensors [4, 12, 14].

However, a nanocomposite sensor with the capability of perceiving high-frequency or ultrahigh-frequency strain signals is still lacking. Ultrahigh-frequency signals, such as ultrasonic waves ($>$20 kHz) or high-frequency vibration or sound signals (around several hundred to several thousand Hertz), usually feature ultra-low magnitude (in the order of microstrain), posing a vast challenge for signal acquisition using conventional nanocomposite sensors [9, 16]. The low-magnitude signals not only lead to an extremely low strain applied on the sensors and thus a low

signal-to-noise ratio (SNR), but also introduce great difficulty for a signal acquisition system to efficiently convert strain to electrical signals. Indeed, the development of flexible strain sensors with sensing capability over a broad band with response to high-frequency signals is of vital importance in many sensing applications including biological motion detection, robotic research and development, and ultrasonic wave-based health monitoring [9, 17-18].

A tunneling effect is often introduced as a sensing mechanism in nanomaterial-based strain sensors. This effect can occur when neighboring building blocks in a nanofiller network are in close proximity (around several nanometers) but not in direct contact [19]. Under externally applied strain, the average distance between two adjacent nanoparticles alters, leading to the tunneling of charged carriers and a consequent increase in local electrical conductivity [4, 19-22]. Therefore, control of the morphology or distribution of the nanoscale building blocks in macroscopic constructions, so as to obtain a desired tunneling effect, may be instrumental in driving strain sensors to become responsive to high-frequency strains with ultra-low magnitude.

Recently, a type of quasi-continuous nanographene film has been developed and used for strain sensors with a high strain GF of 600+, and the tunneling effect between the nanographene was considered the dominant sensing mechanism in the low strain range below 0.3 % [19]. Using both numerical simulation and experimental validation, researchers have argued that the tunneling effect between adjacent nanoparticles in a nanofiller network was the driver that made multi-walled carbon nanotube (MWCNT)/epoxy composite sensors responsive to low strain [23]. That study also highlighted a GF up to 22.4 under 0.6% static strain after optimization of the nanofiller type, diameter, and conductivity of MWCNTs in the sensor [23]. Further optimized metal-coated MWCNT has also been developed and applied to increase sensing sensitivity by improving the conductive network in polymer matrix [24]. The tunneling effect in nanomaterial-based strain

sensors suggests a high potential to perceive broadband signals of high frequency but low magnitude using nanocomposite sensors with optimized nanofiller networks.

Actually, the optimization of a conductive network formed by nanofillers in conductive polymer composites (CPCs) has been extensively investigated for the development of high-performance nanocomposites [25-27]. The dispersion, morphology, and microstructure of the conductive networks in the CPCs can be controlled and optimized to create the desired tunneling effect. Moreover, numerous merits of nanocomposites, derived from coactions between polymer matrix and nanofillers [10, 27], including low density, desired flexibility, easy modifiability in shape and size, chemical stability, low fabrication cost, along with outstanding electrical and mechanical performance, also make CPCs promising candidates for the development of high-performance strain sensors that can respond to broadband strain signals up to the ultrasonic regime [28-30].

Thanks to recent groundbreaking developments in materials science, the rapid response of CPCs to high-frequency ultrasonic waves was explored for the first time in our previous work [31]. However, the sensing mechanism and the factors influencing the sensing performance of the sensor require clarification that is critical for deeper research and development of relevant high-frequency sensors. Moreover, applications and exploration based on such novel sensors are also lacking. As an extension of the previous work and with the aim of gaining insight into the sensing mechanism of the developed sensor's responses to broadband and high-frequency strain signals, in this study we prepared carbon nanostructured polyvinylidene fluoride (PVDF)-based nanocomposites, as typical CPC-type strain sensors, for evaluation of their strain-sensing performance, from static tension and low-frequency cyclic loading, through high-frequency structural vibration, to ultrahigh-frequency ultrasonic guided waves (UGWs) (up to 400 kHz). On the basis of

experimental results and a nanoscale theoretical model, the sensing mechanism of the nanocomposite sensors under ultra-broadband frequency strains is discussed here. Finally, as a proof-of-concept application, the developed sensors are networked to form an *in-situ* sensor network to successfully implement ultrasonic guided-wave-based structural health monitoring (SHM).

2 Experimental

2.1 Fabrication of nanocarbon/PVDF composites: Carbon black (CB) nanofiller (N220, average particle diameter: ~80 nm, supplied by CABOT Co.), MWCNTs with different aspect ratios (TNM8, purity > 95 wt%, average diameter around 50 nm and length 10–20 μm, supplied by Chengdu Institute of Chinese Academy of Sciences; FloTube™ 7000, average tube diameter: ~6–10 nm, length: ~50 μm, aspect ratio: ~5000-8000, purity > 95 wt %, supplied by CNano Technology Ltd.) were used to fabricate the PVDF (Kynar k721, density: 1.74 g/cm^3, melting point: ~158 ºC, ARKEMA) -based composites by standard melt-mixing processes. For each nanofiller type, nanocomposites with various nanofiller-to-matrix mass ratios were fabricated in an internal mixer at 190 ºC and 50 rpm for 0.5 hour. After that, using a standard hot-pressing process (at 20 MPa and 190 ºC for 10 minutes, then cooling to room temperature at atmospheric pressure for another 60 minutes), nanocomposites were immobilized between two steel plates, degassed in vacuum to remove trapped air bubbles, cured for 24 hours at room temperature under atmospheric pressure, and molded to films ~200 μm in thickness.

2.2 Characterization: The microstructure of the composites with various MWCNT and CB contents was investigated by scanning electron microscopy (SEM, JEOL JSM-7500F). The

resistance (R) of the composites was measured by the four-probe method with a Keithley 4200-SCS (semiconductor characterization system) at room temperature. The electrical conductivity (σ) was obtained by the equation $\sigma = l / (R \cdot A)$, where A and l are the effective area and length of the measuring electrode, respectively. At least three film samples for each concentration of nanocomposites were measured and the calculated electrical conductivity of each component indicated a similar value, implying the uniform dispersion state of the conductive carbon nanofillers in the nanocomposites. X-ray diffraction (XRD) measurements for the CB/PVDF composites were carried out at room temperature with specular reflection mode (Cu Ka radiation, X'Pert PRO, PANalytical, Holland).

2.3 Measurement: from quasi-static strains, through vibration, to ultrasonic waves

2.3.1 Quasi-static strain: The electromechanical responses of the PVDF-based nanocomposite sensing elements were evaluated by combining the Keithley SCS results and a dynamic mechanical analysis (DMA, TA Q800). In the electromechanical test, two electrodes were coated with silver paste on one side of the film sensors to measure the resistance that was found to be very similar to the intrinsic resistance of a raw sensor prior to electrode installation. During the tensile process, the resistance of the film sensors was measured simultaneously. At least three samples of the nanocomposite sensors, at each degree of the weight percentage of the nanofiller, were selected to evaluate the electromechanical responses, all showing a similar strain sensitivity (GF) under the given strains applied.

2.3.2 Vibration-induced strain: Owing to the low magnitude of elastic disturbance, signals captured by the sensors were envisaged to be prone to contamination from ambient noise and

uncertainties that under most circumstances would lead to a low SNR. To circumvent this, a self-contained signal amplification and acquisition system was developed for use in conjunction with the sensors. The system contained a signal amplification module and a signal generation/acquisition module, developed on a PXI (PCI eXtensions for Instrumentation) bus platform (NI® PXIe-1071). The amplification module integrated a Wheatstone bridge with resistors compatible with the resistance of the selected sensor (resistance was ascertained via electrical analysis), an electronic amplifier circuit, a series of filters, and a signal conversion unit (for converting measured piezoresistivity to electrical voltage signals). The signal generation/acquisition module consisted of an electromechanical shaker (B&K® 4809) (for introducing vibration to a structure), a linear power amplifier (Ciprian® US-TXP-3), and an oscilloscope (Agilent® DSO9064A). Using these two modules, structural vibration signals were generated and then captured.

A cantilevered glass fiber-epoxy composite beam (290 mm long, 38 mm wide, 2 mm thick) was prepared, to which a nanocomposite sensor and a strain gauge sensor (for comparison) were surface-attached using an instant glue (Aron Alpha® HHI-11485). The central position of the sensor was measured 70 mm from the clamped end of the beam. The shaker excited the beam through a point 270 mm from the clamped end with a sinusoidal signal sweeping between 100 and 3000 Hz. By this means, we examined the feasibility and performance of the fabricated CPC-based sensors for *in-situ* perception of elastic disturbance up to 3000 Hz.

2.3.3 Ultrasonic guided-wave-induced strain: To generate UGWs, numerous lead zirconate titanate (PZT) wafers (Physik Instrumente Co., Ltd., PIC151; diameter: 9 mm; thickness: 0.5 mm) were surface-mounted on a glass fiber-epoxy composite plate (600×600×2 mm^3) using a thin

adhesive layer. The excitation signal – a five-cycle Hanning-window modulated sinusoidal toneburst at various central frequencies – was generated with a waveform generator (NI® PXIE-1071) and then amplified by a linear power amplifier (CIPRIAN® US-TXP-3) to 200 Vp-p before it was applied on individual PZT wafers. Under the excitation, Lamb waves were generated in the composite plate. The same signal acquisition module as that used for the vibration part was adopted, serving an essential role because the elastic disturbance induced by UGWs in a frequency range of kilo- or megaHertz is usually as weak as several microstrains. The Lamb waves were acquired by the PZT and CPC-based composite sensors and recorded by a digital signal oscilloscope (Agilent® DSO9064A) at a sampling rate of 10 MHz. The piezoresistivity of the nanocomposite sensor was reflected by the voltage signal obtained using the developed signal amplification and acquisition system.

In the present study, we focused on evaluation of the sensitivity and ultra-broadband frequency responses of the developed nanocomposite sensors to elastic disturbances (from quasi-static strain to high-frequency ultrasonic waves). The elastic disturbances-induced strains are far lower than the maximal fractured strain of the nanocomposites. In such an elastic region, stretchability would not be a concern. However, more mechanical properties of the nanocomposite sensors including stretchability will be scrutinized in future study.

3 Results and Discussion

3.1 Structures and material properties

The change in resistance of CPCs under external strain relies mainly on the changes in conductive networks, including loss of contact between nanofillers, the tunneling effect originating from the

tiny change in distance between two adjacent nanofillers, and the existing piezoresistivity of nanoscale fillers such as carbon nanotubes, attributed to the chirality and change in barrier height [4, 25]. Nevertheless, the piezoresistivity effect of nanofillers themselves in the composites under external strain was very low, as the large elastic mismatch and weak interfacial strength between nanomaterials and polymer matrix led to negligible deformation of nanomaterials [4, 24, 32]. Thus the change in conductive networks or paths in the polymer matrix was considered the dominant factor leading to the change in resistance of the CPCs under applied strains. This observation confirmed that constructing and optimizing the conductive network in the nanocomposites was essential to obtaining the desired strain sensitivity.

Before comparing the influence of the nanofiller-formed network on the conductivity manifested by a sensor, the influence of PVDF matrix had to be excluded. With the adopted fabrication methodology (i.e., melt-molding, a prevailing nanofiller dispersion technique), XRD of the PVDF-based nanocomposite indicated the dominant alpha crystal type with peaks around 17.7°, 18.4°, and 19.9°, as shown in Fig. 1a, thus no obvious piezoelectric response of the PVDF. Various nanocarbon types, including the long- and medium-aspect ratios of MWCNT (defined as L-MWCNT and M-MWCNT, respectively), and the low-aspect ratio of CB nanofillers, along with various CB contents, indicated the marginal effect on the crystallizing type of the PVDF-based nanocomposites. This finding was important for better understanding of the influence of the nanofiller types and contents on the electromechanical sensing performance, especially for the high-frequency piezoresistive sensing performance discussed in this work. In short, the influence of the PVDF matrix on strain-sensing performance could be excluded and the resistance change in the composites could be ascribed to the change of conductive networks in the polymer matrix [33-36].

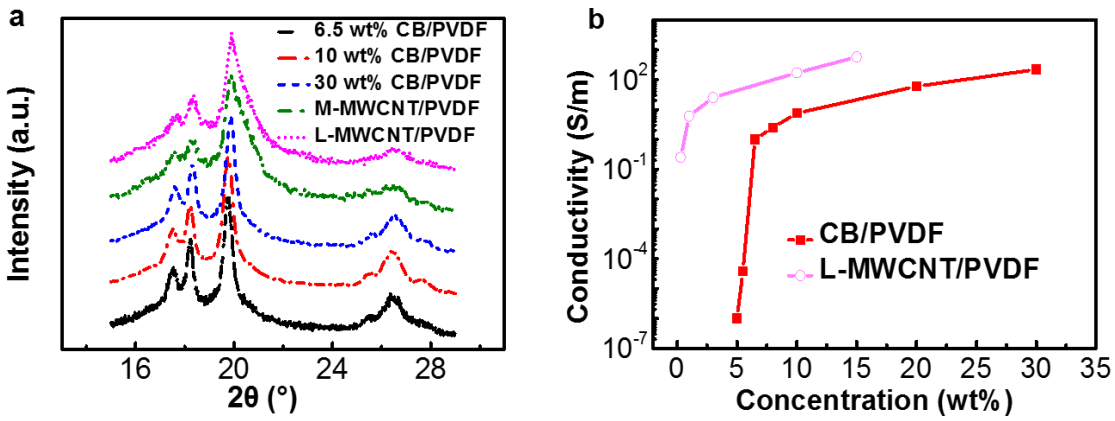

Fig. 1 – (a) XRD patterns of the PVDF-based nanocomposites filled with various nanocarbons and mass ratios of CB nanofillers, (b) electrical conductivity of CB/PVDF and L-MWCNT/PVDF composites with various filler contents.

In the PVDF-based nanocomposites, a higher aspect ratio of carbon nanofillers in the polymer matrix could result in a lower percolation threshold and higher conductivity of nanocomposites with similar content. For example, the percolation thresholds of the CB/PVDF, M-MWCNT, and L-MWCNT nanocomposites were around 6.5 wt%, 2 wt%, and 1 wt%, respectively. Electrical patterns as displayed in Fig. 1b of L-MWCNT/PVDF and CB/PVDF nanocomposites were used to allow detailed comparison that revealed the percolation phenomenon and conductivity with various nanocarbon contents, also implying the dispersion and distribution state of nanofillers in the matrix, as shown in Fig. 2a-d and in our previous report displaying that of nanocomposites with various CB contents [31]. CB nanofillers could be dispersed randomly with small aggregates in the PVDF matrix, and the composites with CB content near the percolation threshold (6.5 wt%) (Fig. 2a,b) showed a sharp increase in conductivity due to the initial formation of conductive paths, resulting in the conversion from insulation to conduction of the nanocomposites. If the CB content increased further, a dense and saturated conductive network was constructed with slowly increasing conductivity [31]. MWCNT/PVDF composites exhibited behaviors similar to those of

CB/PVDF, but more entanglements of MWCNT in the matrix were clearly observed, as exhibited in Fig. 2c, d. Moreover, the coaction between the nanocarbon and PVDF matrix endowed the composites with lightness, good mechanical performance, and flexibility, as shown in Fig. 2e. In particular, the flexibility of the nanocomposites made the sensor adaptive to a curved structural surface – a challenging task difficult for a conventional ceramic-based sensor such as PZT with its relatively high density and rigidity (Fig. 2f). Additionally, those merits also allowed the nanocomposites to be easily patterned on various substrates (Fig. 2g, h), a feature that would be of critical importance for deploying a large-scale sensor network for different purposes such as *in-situ* SHM (detailed in a subsequent section).

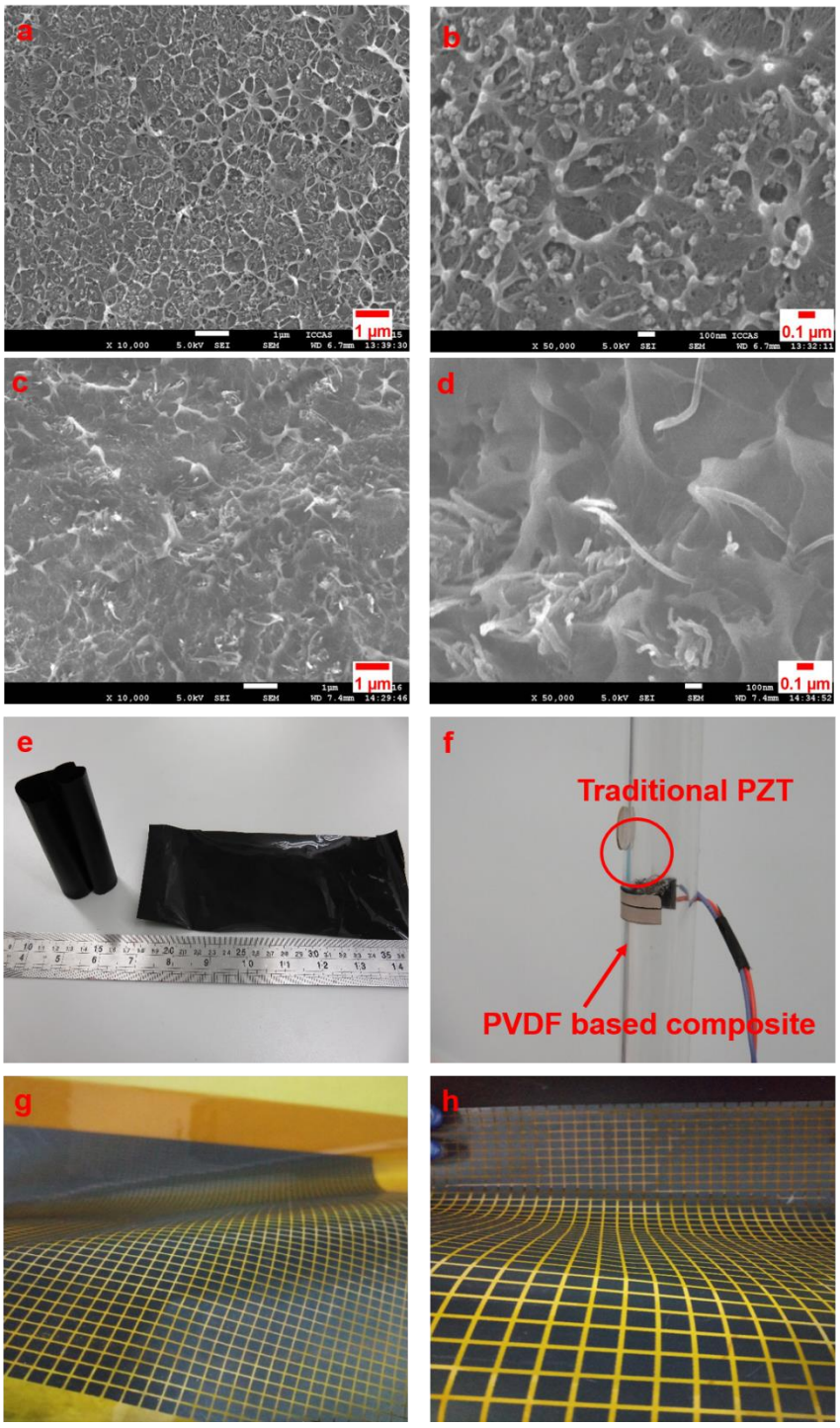

Fig. 2 – SEM images of (a-b) 6.5 wt% CB/PVDF composites and, (c-d) 1.0 wt% L-MWCNT/PVDF composites (scale bars are 1 μm for a, c, 100 nm for b, d), optical images of (e)

the flexible PVDF-based nanocomposites, (f) comparison of the nanocomposites and rigid PZT, (g-h) the PVDF-based nanocomposites patterned on the polyimide substrate.

3.2 Theoretical model

Without loss of generality, Fig. 3 shows the established 3D microscale model with CB as the nanofiller, permitting theoretical study of the piezoresistivity mechanism of the developed PVDF-based nanocomposites. First, according to a standard image analysis process [37], the average number of CB particles within an individual CB aggregate was estimated to be 16, based on microstructural images; the CB aggregates were then assumed to possess fractal geometries, represented by $n \approx C\left(R / r_p\right)^D$, where n is the number of particles and R and r_p are the radius of the CB aggregate and particle, respectively. C and D are the pre-factor and the mass fractal dimension, set at 1 and 1.71, respectively. Such values represented a relatively high level of structural branching [38]; finally, a number of CB aggregates were distributed randomly in a representative volume element (RVE) measuring 2 μm in each dimension.

The aggregate dispersion close to the percolation threshold is presented in Fig. 3a. It can be seen that a conductive path, equivalent to a cluster of CB particles highlighted in red, is formed. This CB cluster could be treated as an equivalent conductive resistor network comprising two types of resistor, as shown in Fig. 3b, *i.e.*, the particle resistor and the resistor associated with the tunneling effects between adjacent particles. The tunneling resistance could be calculated according to [39]

$$R_{Tunneling} = \frac{16\pi^2 h}{3e^2}\frac{d}{k_0 S}\exp\left(k_0 d\right), \qquad (1)$$

where k_0 is the potential barrier in terms of $k_0 = 2\sqrt{2m_eV_e}/h$, in which V_e signifies the potential height of 0.2 eV, m_e is the mass of an electron and h is the Planck constant; e is the elementary charge; d is the gap width between adjacent CB nanoparticles. $d < d_c$ is considered as the condition triggering a tunneling effect, in which d_c, set as 5 nm in the present study, is the critical gap width determined by the level of the potential barrier. The overall resistance of the resistor network was calculated according to Kirchhoff's current law and matrix representation method [4, 19]. Subject to different strain levels of the RVE, the displacement of the CB particles within an individual aggregate was assumed to be equal to that of the mass center of the aggregate, that could be calculated using the coordinate and strain level at the mass center by taking into account the Poisson's ratio of the matrix (0.3 for PVDF). Under a given strain level, the geometry of the conductive CB cluster was reconstructed according to the displacements of all the aggregates, and the network resistance changes were recalculated accordingly.

Static and dynamic piezoresistive responses of the RVE were simulated, and the variations of the resistance change ratio, i.e. $\Delta R/R$, were plotted along with strain variation. In Fig. 3c it can be observed that, subject to a relatively wide range of strain (±1 %), the static piezoresistive response of the RVE exhibits a nonlinear exponential trend. That phenomenon was mainly associated with the exponential variation of tunneling resistance as expressed in Eq. (1), and the contribution from the tunneling effect could be considered dominant under such a strain level (*i.e.*, ±1 %). On the other hand, within a tiny strain sub-range (e.g., a range of $\pm 10\mu\varepsilon$ that is typical of an ultrasound-induced signal), the variation trend of the resistance change ratio could be considered approximately linear. That feature is of great importance for a CB/PVDF sensor in the estimation of quantitative strain.

Periodical dynamic strain excitation was then introduced in the RVE and the piezoresistive responses were calculated and are presented in Fig. 3d. It is important to note that the strain range of ±1 % leads to a markedly asymmetrical response subject to tension and compression, respectively, whereas the range of $\pm 10 \mu\varepsilon$ generates an exactly harmonic response. From the above discussion, it could be realized that the CB/PVDF composite had promising potential in the quantitative measurement of ultrasonic wave signals.

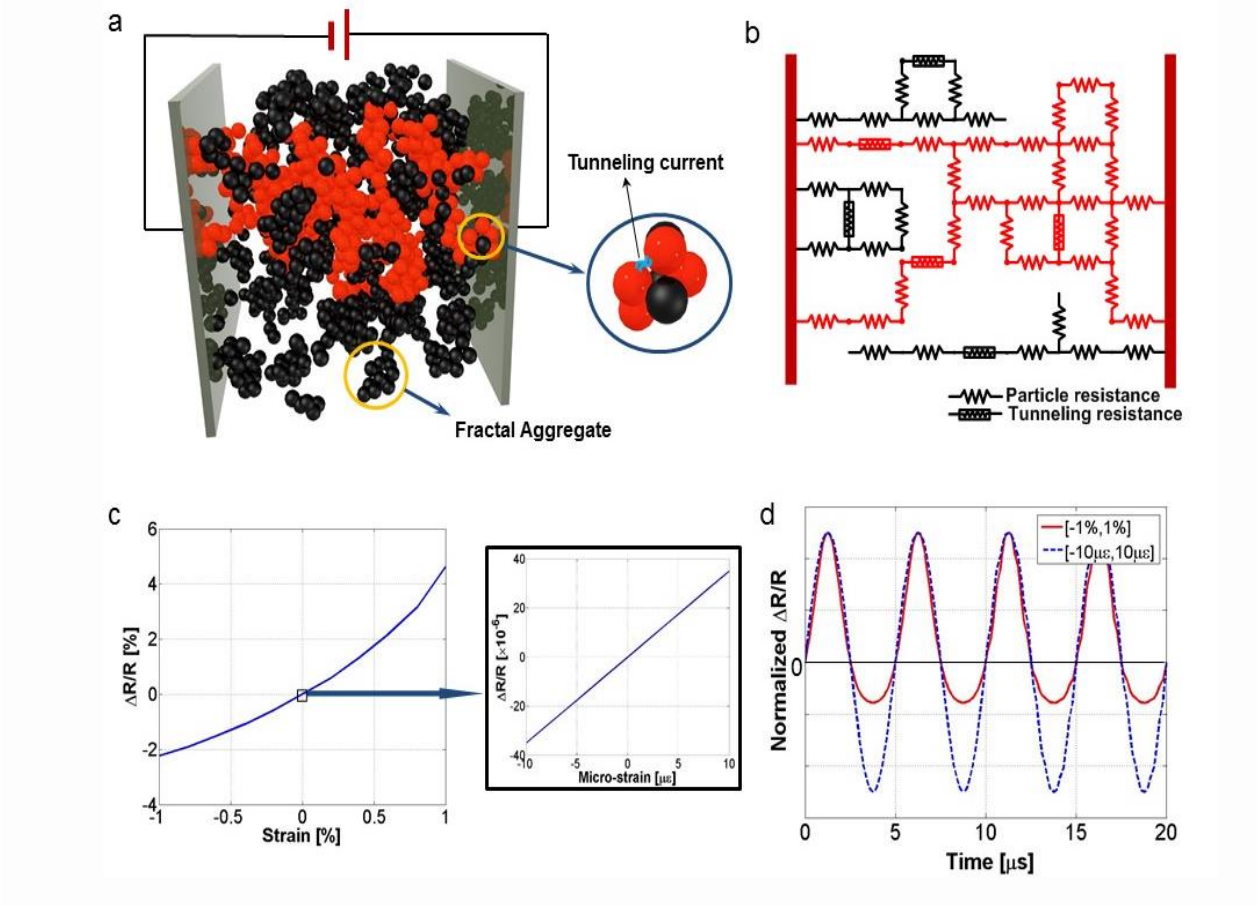

Fig. 3 – (a) Molecular model of CB aggregates dispersed in the RVE, and (b) schematic diagram of the equivalent resistor network of the CB agglomerate, piezoresistive response of the RVE subject to (c) static and (d) dynamic strain variation with 200 kHz frequency under strain range of [-1%, 1%] and [-10 $\mu\varepsilon$,10 $\mu\varepsilon$], respectively.

3.3 Strain-sensing performance

In our previous study [31], it was proved that once its content greatly exceeded the percolation threshold, the nanofiller had little effect on a conductive network that was already dense and saturated. Thus, composites with a further increase in nanofiller content lowered the strain sensitivity or GF [31]. Composites with content around the percolation threshold usually showed the highest GF under static strain, as also reported elsewhere [23-24]. Moreover, various types of nanofiller-based conductive networks also led to different sensing performance, as shown in Fig. 4. Compared with the MWCNT network with more entanglements in the polymer matrix as discussed above, the nano-CB-based conductive network formed more contact points between CB nanofillers, enabling synchronous and precise deformation of the conductive network following external strains. Therefore, various composites with similar conductivity near the percolation threshold were compared under low-frequency cyclic strain with the magnitude of 1%. The CB/PVDF nanocomposites indicated good repeatability and high sensitivity, whereas the MWCNT/PVDF composites showed low sensitivity. Actually, as shown in Fig. 4b, the sensing performance of the M-MWCNT/PVDF nanocomposites near the percolation threshold shows much higher sensing stability than that of the L-MWCNT/PVDF composites, but a lower GF than the CB/PVDF nanocomposites. In short, on the basis of the morphological characterization of the nanofillers with various types and contents, together with detailed strain-sensing analyses of related nanocomposites, the critical roles of the conductive network for the strain-sensing performance of CPCs under static or low-frequency cyclic loadings were well proved.

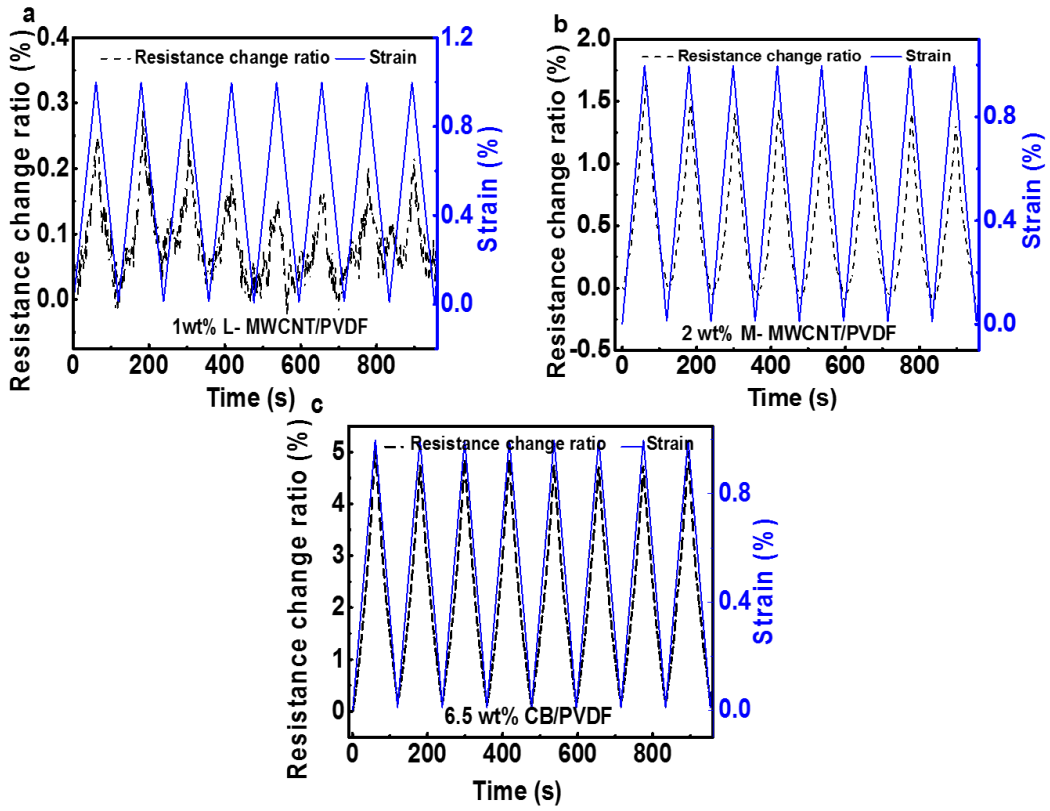

Fig. 4 – Resistance change ratio under low-frequency cyclic tensile loading of the PVDF-based composites with nanocarbon content near the percolation threshold: (a) 1.0 wt% L-MWCNT/PVDF composites, (b) 2 wt% M-MWCNT/PVDF composites, (c) 6.5 wt% CB/PVDF nanocomposite.

On the basis of the foregoing analysis, 6.5 wt% CB/PVDF nanocomposites near the percolation threshold were selected for better understanding of the electromechanical responses of the PVDF-based nanocomposites. Under static strain until material fracture of the nanocomposites, both the resistance change ratio and stress as a function of the tensile strain were analyzed to quantitatively characterize the strain sensitivity, as shown in Fig. 5a. Clearly, high mechanical strength and large fracture strain can be indicated in the flexible composites; the resistance changes immediately with increasing strain. Further, a higher GF is obtained with higher strain: the GF of

the composites is greater than 20 near the fracture strain ~7%. This is consistent with the sensing mechanism of CPCs subject to a large strain: numerous irreversible losses of contact alter the conductive network drastically, and accordingly increase the resistance of the composites. When the applied cyclic strain is below 1%, however, the resistance change is reversible, as indicated in Fig. 5b. Meanwhile, various tensile speeds, corresponding to loading frequencies from ~0.004 to ~0.08 Hz of the composites under 1% strain, are applied as displayed in Fig. 5c. A similar GF ~5 under the low-frequency cyclic strain is obtained, higher than the GF of a traditional metal foil-based strain gauge (GF ~2) due to the distinct microstructures of the nanocomposites. More importantly, the similar GFs can imply that the interfaces between the nanofillers and PVDF matrix are adequate [40], a finding that is also important for the high-frequency electromechanical performance of the PVDF-based nanocomposites.

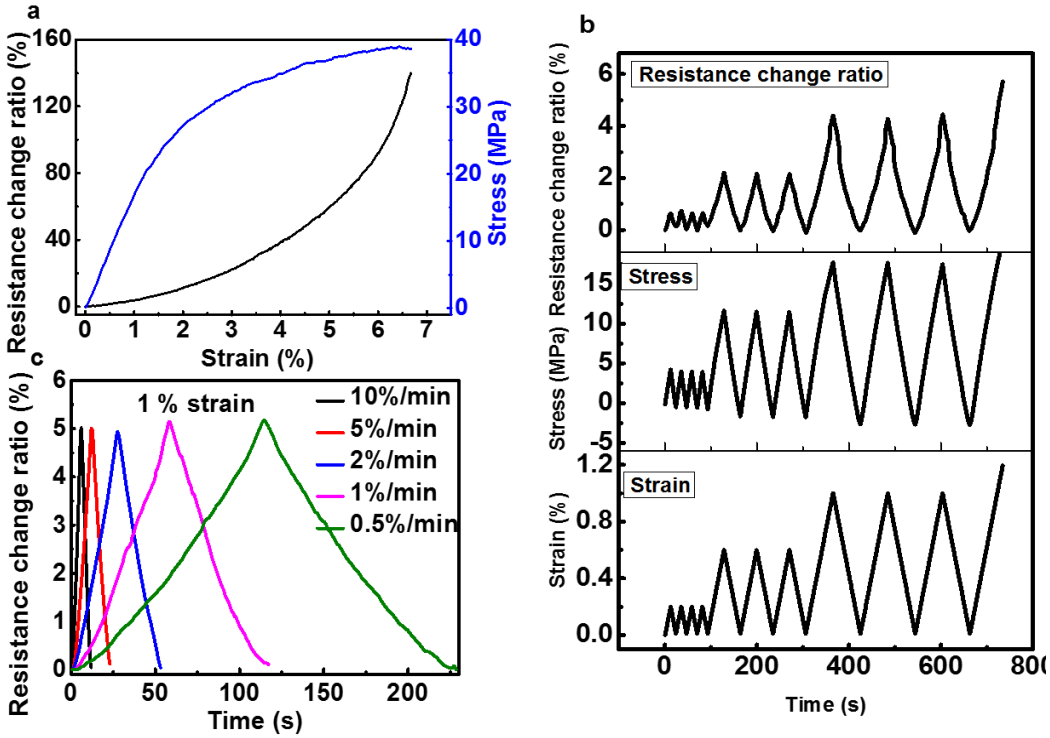

Fig. 5 – Electromechanical response and mechanics of 6.5 wt% CB/PVDF nanocomposites: (a) resistance change ratio and stress of composites under applied strain, (b) cyclic electromechanical

responses of composites under various low strains, (c) resistance change ratio of composites under various tensile speeds.

To better understand the broadband frequency of sensing performance, a sensing performance test of the CPCs under high-frequency vibration was designed. As shown in Fig. 6a, for strain sensing a vibration shaker excites a glass fiber-epoxy beam to which the composite sample is attached. Any change in resistance of the composite is converted to electric signals through a dedicated circuit system whereby a higher amplitude of voltage signals a greater change in the resistance ratio of sensors. As indicated in Fig. 6b, the CB/PVDF nanocomposites show stable, reversible, and repeatable piezoresistive responses under high-frequency vibration from 100 to 3000 Hz. Fig. 6c also shows that by increasing the magnitude of excitation and thus the strain of the nanocomposites, the signals acquired from the CB/PVDF show a rising trend. Further quantitative comparison indicates that for all the composites with various CB contents, the acquired high-frequency sensing signals have a nearly linear correlation with the input excitation voltage (Fig. 6d). Besides, the closer the CB content is to the percolation threshold, the higher are the response signals. Therefore, CB/PVDF nanocomposites near the percolation threshold can also exhibit optimal strain-sensing performance under high-frequency vibration, compared with nanocomposites filled with other CB contents or MWCNTs, as well as the metal-based strain gauge (Fig. 6d, e). The consistency between the high-frequency and low-frequency sensing performance of the PVDF-based nanocomposites further demonstrates the critical roles that the conductive network plays in broad-frequency strain-sensing performance.

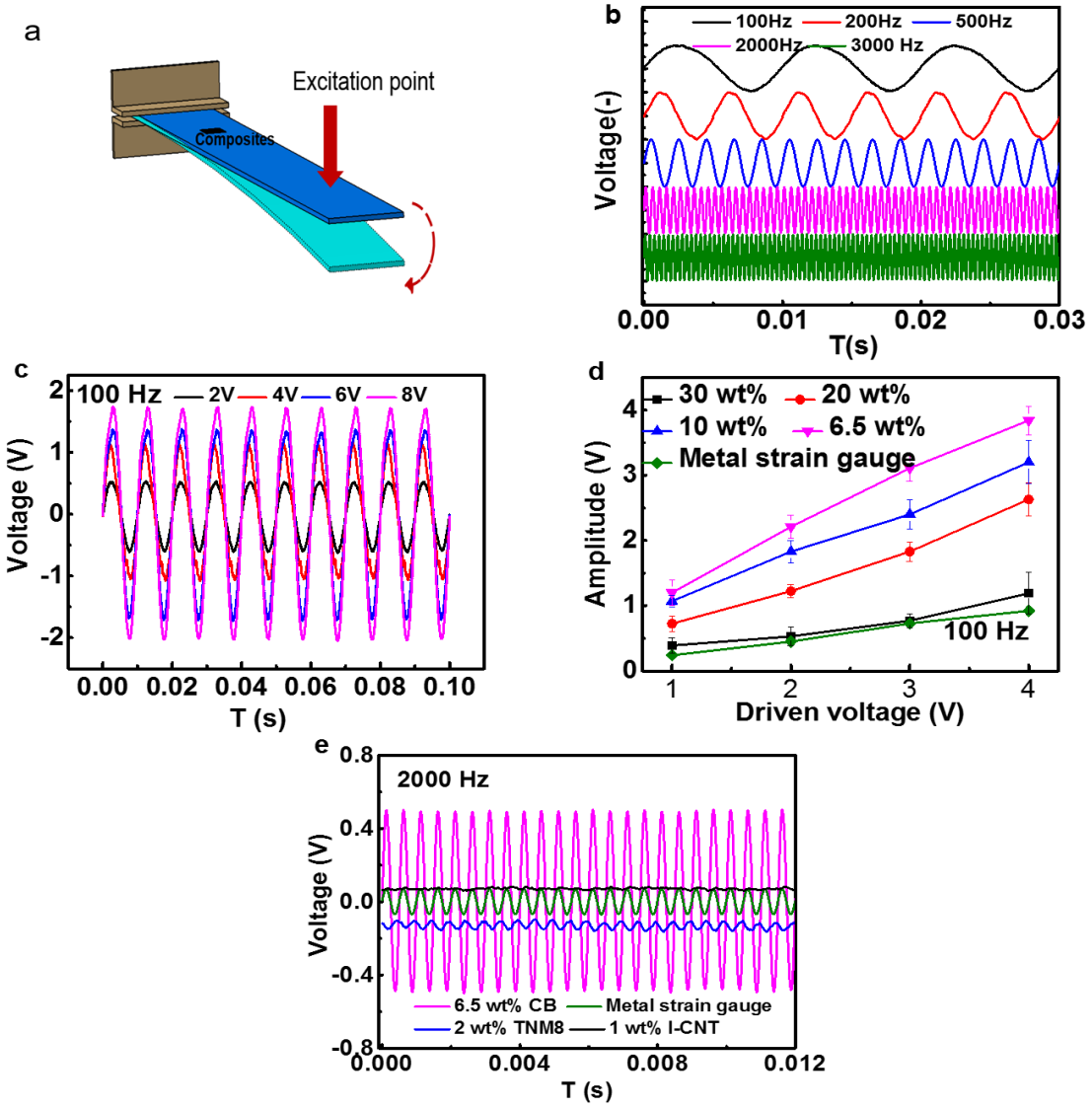

Fig. 6 – Sensing response of PVDF-based nanocomposites under high-frequency vibration: (a) schematic images of the test setup, (b) normalized response signals of 6.5 wt% CB/PVDF nanocomposite subject to excitation frequencies from 100 to 3000 Hz, (c) response signals of 6.5 wt% CB/PVDF composites under 100 Hz frequency of vibration with various excitation magnitudes, (d) amplitudes of sensing signal for various concentrations of CB/PVDF composites under various excitation magnitudes at 100 Hz, (e) response signals of PVDF-based

nanocomposites (MWCNT/PVDF and CB/PVDF nanocomposites) and metal-based strain gauge under the same vibration frequency (2000 Hz) and driven voltage.

To explore in depth the electromechanical response mechanism of the PVDF-based nanocomposites, the dynamic mechanical performance under various frequencies was obtained. As indicated in Fig. 7, the variation pattern of the PVDF-based nanocomposites is similar to that of the typical 6.5 wt% CB/PVDF nanocomposites. The storage modulus increases while the loss modulus (and tan delta, indicating the ratio of energy dissipated to energy stored in the deformation cycle) decreases slightly with increasing frequency, indicating that the nanocomposites could maintain their elastic performance with insignificant viscosity under high-frequency conduction [18]. Thus, a reliable mechanical response of the carbon nanostructured PVDF composites to high-frequency strain can be expected, which, combined with the repeatability of sensing shown under more than 400 cycles of low-frequency strain (~ 0.08 Hz) as shown in Fig. 8a, endow the nanocomposites with promising high-frequency strain-sensing performance. Notably and importantly, more than 100 million (10^8) repeated cycles under the vibration of 3000 Hz are implanted, as indicated in Fig. 8b, not only testifying to the durability and stability of the composites for practical applications under high-frequency vibration, but also showing consistency with the analysis of the dynamic mechanical performance. SEM images of the CB/PVDF nanocomposites obtained before and after cyclic testing show no distinguishable morphological change – a finding consistent with the reversible resistance change behavior of the nanocomposites.

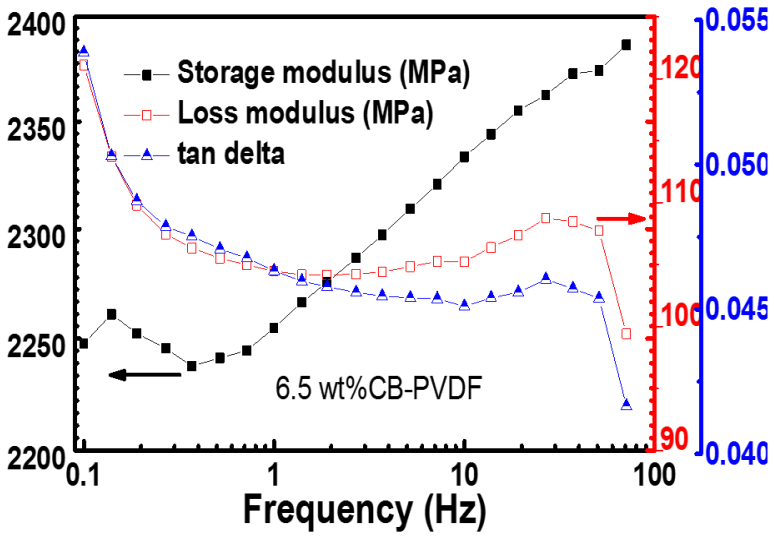

Fig. 7 – Dynamic mechanical analysis of the nanocomposites under various frequencies.

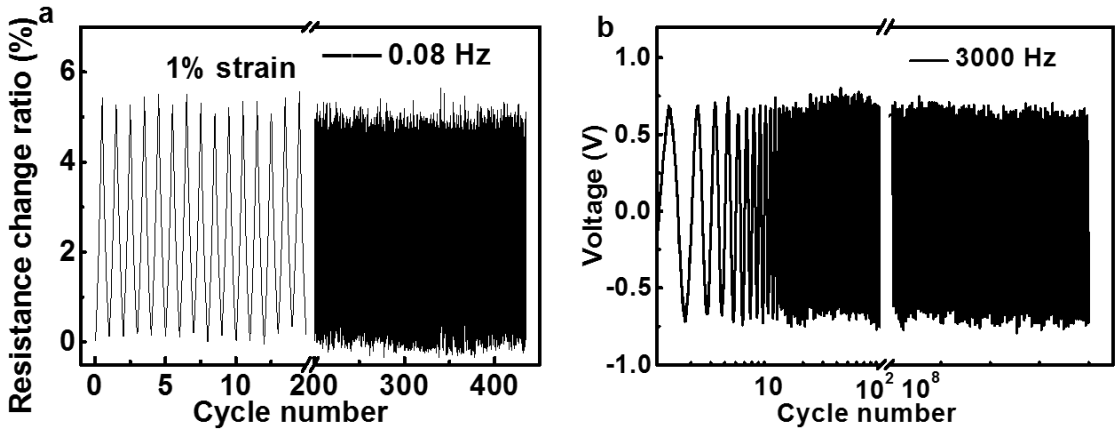

Fig. 8 – Cyclic testing of the 6.5 wt% CB/PVDF nanocomposites under different frequencies: (a) low strain with 10%/min tensile speed (~ 0.08 Hz) and (b) long cyclic sensing test (more than 100 million cycles) under high-frequency vibration (3000 Hz).

Although the sensing ability of the CB/PVDF nanocomposites to high-frequency UGWs (around 175 kHz) was simply realized in our previous report [31], systemic research into the

mechanism has been lacking. To better understand sensing performance and to further explore the sensing frequency limit of the piezoresistive CPCs, PVDF-based nanocomposites filled with various types and concentrations of carbon nanofillers were selected as typical CPCs to explore the sensing performance and mechanism of their response to strain signals over a broad frequency range. The knowledge obtained is important for designing other types of CPCs as suitable broadband frequency responsive piezoresistive sensors. With its use of extremely weak wave amplitudes (~10 microstrains), our experiment design and circuit optimization hold great significance for quantitative sensing characterization of CB/PVDF, as shown in Fig. 9a. Through the inverse piezoelectric effect [41-43], a PZT wafer (denoted by PZT_1) generates a high-frequency vibration that propagates as UGWs in a glass fiber-epoxy composite plate and is then acquired by PVDF-based nanocomposites. The experiment uses PZT_2 as the control group against the nanocomposite sensors. As the UGWs propagate in the plate structure omni-directionally with the same velocity, different wave propagation distances correspond to different arrival times of waves. The acquired signals as shown in Fig. 9b show the same arrival time for PZT_2 and 6.5 wt% CB/PVDF nanocomposites, a finding that validates the sensing ability of CB/PVDF to ultrasound at 200 kHz. The crosstalk in the sensing signals of CB/PVDF that appears simultaneously with the excitation is attributed to the imperfect electro-magnetic shielding against the high voltage input to PZT_1, as indicated in our previous report [31]. As also indicated in Fig. 9b, compared with the sensing response of the CB/PVDF nanocomposite near percolation content, the sensing response of the metal-based strain gauge under UGWs, the CNT/PVDF composites (both L-MWCNT and M-MWCNT filled PVDF composites) or the CB/PVDF nanocomposites with too high CB concentrations (30 wt%) is also obtained but is too weak to be detected under the same condition in our systems. This finding can also be attributed to the low strain GF of those sensors, as

discussed above. The findings further verify that, to ensure the high-frequency strain-sensing performance of CPCs, essential prerequisites are both (a) an excellent mechanical response of the polymer matrix and (b) satisfactory sensitivity (or GF) derived from the deformation of the conductive network (especially the tunneling effect) under low-frequency strain.

Generally, ceramic sensing blocks (such as PZT) are widely used as piezoelectric sensors in sensing applications with high SNR, where they are subject to several constraints including rigidity, high density and cost, difficult processing, and proneness to electrical interference [25, 42]. Free from those restrictions, in this work, lightweight and flexible CB/PVDF nanocomposite sensors are shown capable of perceiving UGW signals through a frequency sweeping test from 50 to 400 kHz, with PZT sensors for comparison of time-frequency-magnitude responses, as displayed in Fig. 9c and 9d. The same trends in variation of amplitude are observed from the response signals acquired with both CB/PVDF and PZT sensors in this wide frequency range, proving that the intrinsic perception ability of CB/PVDF up to an ultrahigh-frequency range (400 kHz) can be realized, in conjunction with the use of a dedicated signal acquisition system which amplifies weak strain responses. The nanocomposite and PZT sensors are both observed to reach a response peak at 200 kHz within the discussed frequency range – a property known as “mode tuning” (i.e., the magnitude of the sensor response varies subject to the excitation frequency) [44, 45]. It is worth noting that the amplitude of the piezoresistive sensor is lower than that of the piezoelectric PZT, a finding attributed to the different sensing mechanism [31]. However, the sensing amplitude under high-frequency strain can be further increased by improving the GF of the piezoresistive sensors. Importantly, the strain-sensing frequency range of the piezoresistive CPCs is much expanded in this work and is far greater than that of other piezoresistive strain sensors ever reported, as shown in Table 1. In summary, combining their sensitivity under various strain frequencies as

demonstrated, with the advantages of flexibility, lightness, low cost, and easy processing or shaping, the CPCs based sensors exhibited excellent potential for sensing applications that require various frequency regions, such as in the detection of ultrahigh-frequency strain signals.

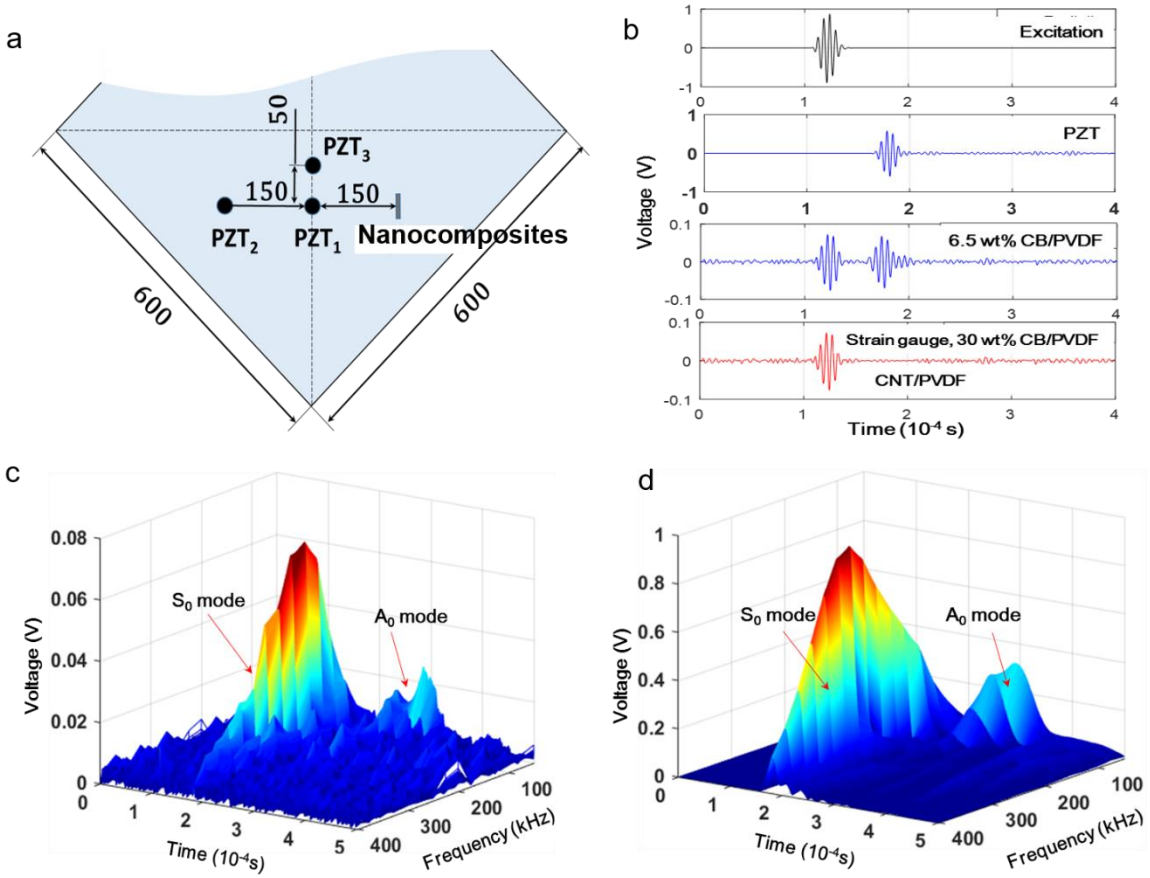

Fig. 9 - Sensing responses of PVDF-based nanocomposites to ultrasonic waves of ultrahigh-frequency: (a) schematic images of test setup, (b) response signals of PZT, 6.5 wt% and 30 wt% CB/PVDF nanocomposite, CNT/PVDF, and metal-based strain gauge subject to the excitation frequency of 200 kHz of ultrasonic guided wave, (c) comparison of time-frequency-magnitude response signals for 6.5 wt% CB/PVDF composites under various UGW frequencies, and (d) similar comparison of time-frequency-magnitude response signals for PZT.

Table 1. Reported frequency sensitivity of existing piezoresistive strain sensors

Reference	Material	Response frequency	Notes
The current study	**CB/PVDF nanocomposite**	**0~ 400 kHz**	Tension, vibration, ultrasonic
Adv. Mater. 2016 [18]	Graphene foam	2 kHz	vibration
ACS A.M.I. 2016 [46]	Micro-cracked graphite -elastomer	99 Hz	sound wave
ACS Nano 2015 [5]	Graphene woven micro-fabrics	100 Hz	acoustic vibration
ACS Nano 2015 [6]	Graphene /PI foam	0.167 Hz	cyclic compression
ACS A.M.I. 2015 [47]	AuNW/PANI-rubber	1 Hz	
Carbon 2015 [28]	CNF/PU nanocomposite	0.0125 Hz	cyclic tension
Nature 2014 [1]	Pt-PDMS	200 Hz vibration ＜ 2 kHz sound wave	crack-based sensor
ACS Nano 2014 [9]	Graphene-rubber composite	160 Hz	vibration
Nanoscale 2013 [48]	Hierarchical graphene foam	0.4 Hz	cyclic compression
Adv. Mater. 2011 [49]	ZnO nanowire/PDMS	2 Hz	
Nat. Nanotechnol. 2011 [2]	Aligned CNT-PDMS	/	breathing response
Carbon 2011 [29]	Aligned CNT/PSF composite	~0.01 Hz	

/: not mentioned or not clear

3.4 Demonstration of high-frequency sensing applications

Finally, *in-situ* ultrasonic wave-based SHM was implemented based on the sensing performance of 6.5 wt% CB/PVDF nanocomposites under the ultrahigh-frequency of UGWs. One PZT wafer was selected for excitation, generating UGWs on a glass fiber-epoxy composite plate, and a composite sensor-based network (300 mm × 300 mm) with eight CB/PVDFs was constructed as shown in Fig. 10a-b. The lightweight composite sensors exerted little weight on the host structure. Then, the generated UGWs were respectively acquired by the eight CB/PVDF nanocomposite sensors. A delay-and-sum imaging algorithm based on the extracted active UGWs using wavelet transform was applied [50]. The excitation central frequency of 200 kHz was chosen for damage imaging, as it was observed that through a frequency sweeping test (Fig. 9c), the S_0 mode at 200 kHz had the greatest signal amplitude. Generally speaking, a probing wave of high frequency and large amplitude is preferred for damage detection. As shown in Fig. 10c, the typical damage imaging result intuitively presents the true damage locations, demonstrating that the developed CB/PVDF sensors can be networked for UGW-based damage detection and other high-frequency sensing applications. More importantly, as presented in Fig. 10d, the flexibility of the nanocomposites is also critical for sensing applications where the monitored structure is not flat. In other words, the demonstrated good performance of these sensors, combined with their potential for printing or patterning in large-area production as discussed above, indicates the great promise for the CPCs to satisfy various applications including the construction of diverse sensor networks for SHM. In order to explore the full potential of nanocomposites in sensing applications, more fundamental science and materials technological advances are also currently under development for sensing scenarios in a wider domain of applications, including developing more polymer or

nanofiller types to accommodate different sensing requirements, and increasing the GF through improving the dispersion of nanoscale units or improving interfaces with polymer matrices.

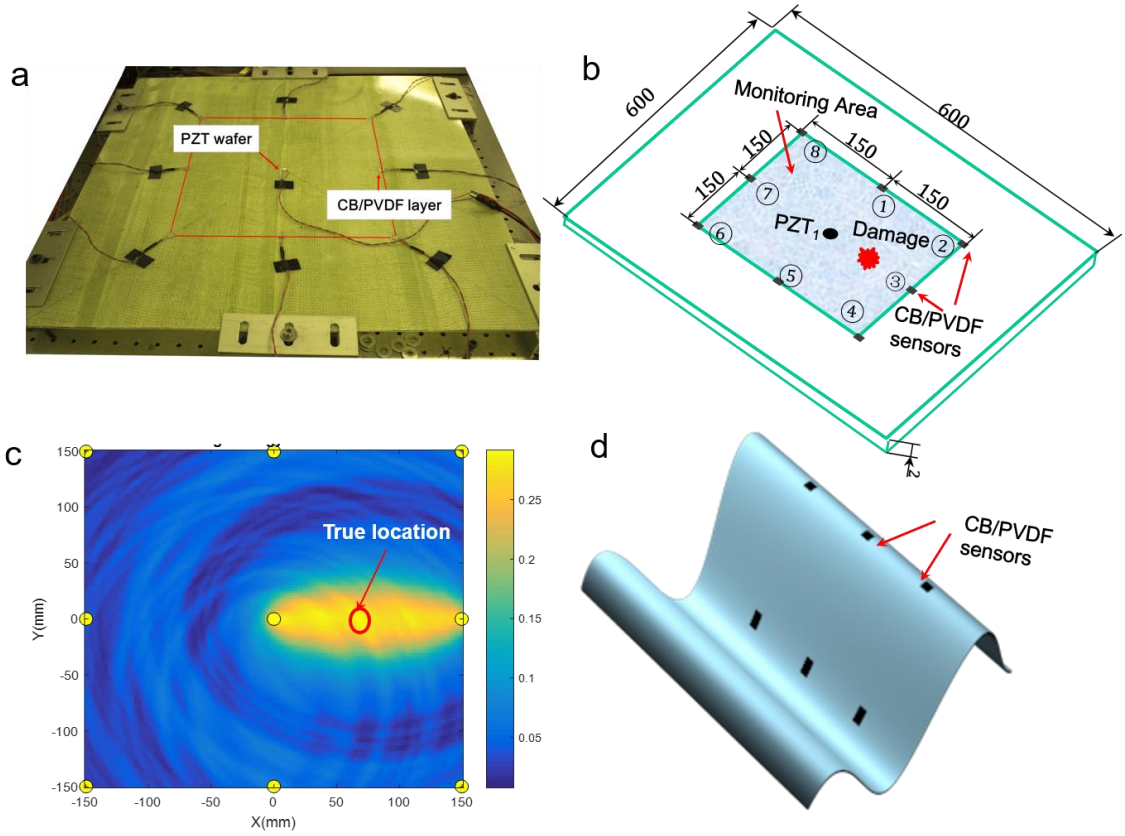

Fig. 10 – *In-situ* UGW-based structural monitoring based on a 6.5 wt% CB/PVDF composite sensor network: (a) optical image and (b) setup of the sensor network, (c) image of the structural state based on the composite sensor network, and (d) proposed sensing applications for a flexible strain sensor network.

4 Conclusions

A type of carbon nanostructured PVDF-based composite sensor was designed and fabricated by a low-cost, and simple fabrication process, showing excellent mechanical flexibility. Experiments and theoretical modeling validated the piezoresistive strain-sensing performance of the sensor

under an ultra-broadband frequency regime (0 ~ 400 kHz), from static and low-frequency cyclic tensile loadings through high-frequency vibration to ultrahigh-frequency UGWs, a range far wider than ever previously reported for a piezoresistive sensor. The influence of the content and type of carbon nanofiller on the sensing mechanism, manifested through the microstructure of the conductive network, was investigated in terms of electrical properties, electromechanical responses, and dynamic mechanisms. A tunneling effect was introduced into a nanofiller conductive network formed in the nanocomposites under applied strain, inducing a dynamic alteration in the piezoresistivity of the sensor. The good mechanical responses of the polymer nanocomposites under high-frequency strain and the satisfactory sensitivity of the sensor under extremely low strain endowed the CB/PVDF nanocomposite sensor with high-frequency strain-sensing performance. Finally, a sensor network based on lightweight flexible CB/PVDF nanocomposites was constructed to successfully implement ultrasonic guided wave-based *in-situ* SHM, indicating excellent application potential of the sensor in ultra-broadband and high-frequency-responsive flexible strain-sensing.

Acknowledgements

This project is supported by the Hong Kong Research Grants Council via General Research Fund (No. 15214414 and 15201416), and by the Hong Kong Innovation and Technology Commission via its Innovation and Technology Fund (No. ITS/058/14).

References

[1] Kang D, Pikhitsa PV, Choi YW, Lee C, Shin SS, Piao L, et al. Ultrasensitive mechanical crack-based sensor inspired by the spider sensory system. Nature 2014, *516*, 222-6.

[2] Yamada T, Hayamizu Y, Yamamoto Y, Yomogida Y, Izadi-Najafabadi A, Futaba DN. A stretchable carbon nanotube strain sensor for human-motion detection. Nat Nanotechnol 2011, *6* , 296-301.

[3] Mannsfeld SCB, Tee BCK, Stoltenberg RM, Chen CVHH, Barman S, Muir BVO. Highly sensitive flexible pressure sensors with microstructured rubber dielectric layers. Nat Mater 2010, *9*, 859-864.

[4] Amjadi M, Kyung KU, Park I, Sitti M. Stretchable, Skin-Mountable, and Wearable Strain Sensors and Their Potential Applications: A Review. Adv Funct Mater 2016, 26, 1678-1698.

[5] Yang T, Wang W, Zhang H, Li X, Shi J, He Y, et al. Tactile Sensing System Based on Arrays of Graphene Woven Microfabrics: Electromechanical Behavior and Electronic Skin Application. ACS Nano 2015, *9*, 10867-10875.

[6] Qin Y, Peng Q, Ding Y, Lin Z, Wang C, Li Y, et al. Lightweight, Superelastic, and Mechanically Flexible Graphene/Polyimide Nanocomposite Foam for Strain Sensor Application. ACS Nano 2015, *9*, 8933-8941.

[7] Sebastian J, Schehl N, Bouchard M, Boehle M, Li L, Lagounov A, et al. Health monitoring of structural composites with embedded carbon nanotube coated glass fiber sensors. Carbon 2014, *66*, 191-200.

[8] Wang Y, Wang L, Yang T, Li X, Zang X, Zhu M, et al. Wearable and Highly Sensitive Graphene Strain Sensors for Human Motion Monitoring. Adv Funct Mater 2014, 24, 4666-4670.

[9] Boland CS, Khan U, Backes C, O'Neill A, McCauley J, Duane S, et al. Sensitive, High-Strain, High-Rate Bodily Motion Sensors Based on Graphene–Rubber Composites. ACS Nano 2014, 8, 8819-8830.

[10] Yazdani H, Hatami K, Khosravi E, Harper K, Grady BP. Strain-sensitive conductivity of carbon black-filled PVC composites subjected to cyclic loading. Carbon 2014, 79, 393-405.

[11] Wang W, Yang T, Zhu H, Zheng Q. Bio-inspired mechanics of highly sensitive stretchable graphene strain sensors. Appl Phys Lett 2015, 106, 171903.

[12] Boland CS, Khan U, Ryan G, Barwich S, Charifou R, Harvey A, et al. Sensitive electromechanical sensors using viscoelastic graphene-polymer nanocomposites. Science 2016, 354, 1257-1260.

[13] Liu X, Tang C, Du X, Xiong S, Xi S, Liu Y, et al. A highly sensitive graphene woven fabric strain sensor for wearable wireless musical instruments. Mater Horiz 2017, DOI: 10.1039/C7MH00104E.

[14] Lin Y, Liu S, Chen S, Wei Y, Dong X, Liu L, et al. A highly stretchable and sensitive strain sensor based on graphene–elastomer composites with a novel double-interconnected network. J Mater Chem C 2016, *4* (26), 6345-6352.

[15] Liu Q, Chen J, Li Y, Shi G. High-Performance Strain Sensors with Fish-Scale-Like Graphene-Sensing Layers for Full-Range Detection of Human Motions. ACS nano 2016, 10 (8), 7901-7906.

[16] Putkis O, Dalton RP, Croxford AJ. The influence of temperature variations on ultrasonic guided waves in anisotropic CFRP plates. Ultrasonics 2015, 60, 109-116.

[17] Wei F, Pizhong Q. Vibration-based Damage Identification Methods: A Review and Comparative Study. Struct Health Moni 2010, 10, 83-111.

[18] Qiu L, Bulut CM, Tang Y, Liu JZ, Alan T, Ding J, et al. Ultrafast Dynamic Piezoresistive Response of Graphene-Based Cellular Elastomers. Adv Mater 2016, 28, 194-200.

[19] Zhao J, Wang, G, Yang R, Lu X, Cheng M, He C, et al. Tunable Piezoresistivity of Nanographene Films for Strain Sensing. ACS Nano 2015, 9, 1622-1629.

[20] Zhao J, He C, Yang R, Shi Z, Cheng M, Yang W, et al. Ultra-sensitive strain sensors based on piezoresistive nanographene films. Appl Phys Lett 2012, 101, 063112.

[21] Hu N, Karube Y, Yan C, Masuda Z, Fukunaga H. Tunneling effect in a polymer/carbon nanotube nanocomposite strain sensor. Acta Mater 2008, 56, 2929-2936.

[22] Li C, Thostenson ET, Chou TW. Dominant role of tunneling resistance in the electrical conductivity of carbon nanotube–based composites. App. Phys Lett 2007, 91, 223114.

[23] Hu N, Karube Y, Arai M, Watanabe T, Yan C, Li Y, et al. Investigation on sensitivity of a polymer/carbon nanotube composite strain sensor. Carbon 2010, 48, 680-687.

[24] Hu N, Itoi T, Akagi T, Kojima T, Xue J, Yan C, et al. Alamusi, Ultrasensitive strain sensors made from metal-coated carbon nanofiller/epoxy composites. Carbon 2013, 51, 202-212.

[25] Kanoun O, Muller C, Benchirouf A, Sanli A, Dinh TN, Al-Hamry A, et al. Flexible carbon nanotube films for high performance strain sensors. Sensors 2014, 14, 10042-71.

[26] Deng H, Lin L, Ji M, Zhang S, Yang M, Fu Q. Progress on the morphological control of conductive network in conductive polymer composites and the use as electroactive multifunctional materials. Prog Polym Sci 2014, 39 (4), 627-655.

[27] Zeng Z, Jin H, Chen M, Li W, Zhou L, Zhang Z. Lightweight and Anisotropic Porous MWCNT/WPU Composites for Ultrahigh Performance Electromagnetic Interference Shielding. Adv Funct Mater 2016, 26 (2), 303-310.

[28] Tallman TN, Gungor S, Wang KW, Bakis CE. Tactile Imaging and Distributed Strain Sensing in Highly Flexible Carbon Nanofiber/Polyurethane Nanocomposites. Carbon 2015, 95, 485-493.

[29] Oliva-Avilés AI, Avilés F, Sosa V. Electrical and piezoresistive properties of multi-walled carbon nanotube/polymer composite films aligned by an electric field. Carbon 2011, 49, 2989-2997.

[30] Kong JH, Jang NS, Kim SH, Kim JM. Simple and rapid micropatterning of conductive carbon composites and its application to elastic strain sensors. Carbon 2014, 77, 199-207.

[31] Zeng Z, Liu M, Xu H, Liu W, Liao Y, Jin H, et al. A coatable, light-weight, fast-response nanocomposite sensor for thein situacquisition of dynamic elastic disturbance: from structural vibration to ultrasonic waves. Smart Mater Struct 2016, 25, 065005.

[32] Luo S, Liu T. Structure–property–processing relationships of single-wall carbon nanotube thin film piezoresistive sensors. Carbon 2013, 59, 315-324.

[33] Tang XG, Hou M, Zou J, Truss R, Yang M, Zhu Z. Toughening and reinforcement of poly(vinylidene fluoride) nanocomposites with “bud-branched” nanotubes. Compos Sci Technol 2012, 72, 263-268.

[34] Chang C, Tran VH, Wang J, Fuh YK, Lin L. Direct-write piezoelectric polymeric nanogenerator with high energy conversion efficiency. Nano Lett 2010, 10, 726-31.

[35] Lou Z, Chen S, Wang L, Jiang K, Shen G. An ultra-sensitive and rapid response speed graphene pressure sensors for electronic skin and health monitoring. Nano Energy 2016, 23, 7-14.

[36] Sharma M, Singh MP, Srivastava C, Madras G, Bose S. Poly(vinylidene fluoride)-Based Flexible and Lightweight Materials for Attenuating Microwave Radiations. ACS Appl Mater Inter 2014, 6, 21151-21160.

[37] ASTM D3849-02 – Standard test method for carbon black – morphological characterization of carbon black using electron microscopy (2002) testing method

[38] Klüppel M, Heinrich G. Fractal Structures in Carbon Black Reinforced Rubbers. Rubber Chem Technol 1995, 68 (4), 623-651.

[39] Meier JG, Klüppel M. Carbon Black Networking in Elastomers Monitored by Dynamic Mechanical and Dielectric Spectroscopy. Macromol Mater Eng 2008, 293 (1), 12-38.

[40] Li X, Yang T, Yang Y, Zhu J, Li L, Alam F, et al. Large-Area Ultrathin Graphene Films by Single-Step Marangoni Self-Assembly for Highly Sensitive Strain Sensing Application. Adv Funct Mater 2016, 26, 1322

[41] Dagdeviren C, Su Y, Joe P, Yona R, Liu Y, Kim YS, et al. Conformable amplified lead zirconate titanate sensors with enhanced piezoelectric response for cutaneous pressure monitoring. Nat Commun 2014, 5, 4496.

[42] Xiao P, Yi N, Zhang T, Huang Y, Chang H, Yang Y, et al. Construction of a Fish-like Robot Based on High Performance Graphene/PVDF Bimorph Actuation Materials. Adv Sci 2016, doi: 10.1002/advs.201500438.

[43] Shung KK, Cannata JM, Zhou QF. Piezoelectric materials for high frequency medical imaging applications: A review. J Electroceramics 2007, 19, 141-147.

[44] Giurgiutiu V. Tuned Lamb wave excitation and detection with piezoelectric wafer active sensors for structural health monitoring. J Intel Mat Syst Str 2005, 16, 291-305.

[45] Santoni GB, L. Yu L, Xu B, Giurgiutiu V. Lamb wave-mode tuning of piezoelectric wafer active sensors for structural health monitoring. J Vib Acoust 2007, 129, 752-762.

[46] Amjadi M, Turan M, Clementson CP, Sitti M. Parallel Microcracks-based Ultrasensitive and Highly Stretchable Strain Sensors. ACS Appl Mater Inter 2016, *8*, 5618-26.

[47] Gong S, Lai DT, Wang Y, Yap LW, Si KJ, Shi Q, et al. Tattoolike Polyaniline Microparticle-Doped Gold Nanowire Patches as Highly Durable Wearable Sensors. ACS Appl Mater Inter 2015, 7, 19700-8.

[48] Kuang J, Liu L, Gao Y, Zhou D, Chen Z, Han B, et al. A hierarchically structured graphene foam and its potential as a large-scale strain-gauge sensor. Nanoscale 2013, 5, 12171.

[49] Xiao X, Yuan L, Zhong J, Ding T, Liu Y, Cai Z, et al. High-strain sensors based on ZnO nanowire/polystyrene hybridized flexible films. Adv Mater 2011, 23, 5440-4.

[50] Ihn JB, Chang FK. Pitch-catch Active Sensing Methods in Structural Health Monitoring for Aircraft Structures. Struct Health Monit 2008, 7, 5-19.